

## Original Research

# p53/FBXL20 axis negatively regulates the protein stability of PR55 $\alpha$ , a regulatory subunit of PP2A Ser/Thr phosphatase



Lepakshe S.V. Madduri<sup>a</sup>; Nichole D. Brandquist<sup>a</sup>;  
Chitra Palanivel<sup>a</sup>; Geoffrey A. Talmon<sup>c</sup>;  
Michael J. Baine<sup>a,b</sup>; Sumin Zhou<sup>a</sup>; Charles A. Enke<sup>a</sup>;  
Keith R. Johnson<sup>b,d,e,f</sup>; Michel M. Ouellette<sup>b,g</sup>;  
Ying Yan<sup>a,b,\*</sup>

<sup>a</sup>Department of Radiation Oncology, University of Nebraska Medical Center, 986850 Nebraska Medical Center, Omaha, NE 68198-6850, USA

<sup>b</sup>Department of Biochemistry and Molecular Biology, University of Nebraska Medical Center, Omaha, NE, USA

<sup>c</sup>Department of Pathology and Microbiology, University of Nebraska Medical Center, Omaha, NE, USA

<sup>d</sup>College of Dentistry-Oral Biology, University of Nebraska Medical Center, Omaha, NE, USA

<sup>e</sup>Eppley Institute for Research in Cancer and Allied Diseases, University of Nebraska Medical Center, Omaha, NE, USA

<sup>f</sup>Department of Genetics, Cell Biology, and Anatomy, University of Nebraska Medical Center, Omaha, NE, USA

<sup>g</sup>Department of Internal Medicine, University of Nebraska Medical Center, Omaha, NE, USA

## Abstract

We have previously reported an important role of PR55 $\alpha$ , a regulatory subunit of PP2A Ser/Thr phosphatase, in the support of critical oncogenic pathways required for oncogenesis and the malignant phenotype of pancreatic cancer. The studies in this report reveal a novel mechanism by which the p53 tumor suppressor inhibits the protein-stability of PR55 $\alpha$  via FBXL20, a p53-target gene that serves as a substrate recognition component of the SCF (Skp1\_Cullin1\_F-box) E3 ubiquitin ligase complex that promotes proteasomal degradation of its targeted proteins. Our studies show that inactivation of p53 by siRNA-knockdown, gene-deletion, HPV-E6-mediated degradation, or expression of the loss-of-function mutant p53<sup>R175H</sup> results in increased PR55 $\alpha$  protein stability, which is accompanied by reduced protein expression of FBXL20 and decreased ubiquitination of PR55 $\alpha$ . Subsequent studies demonstrate that knockdown of FBXL20 by siRNA mimics p53 deficiency, reducing PR55 $\alpha$  ubiquitination and increasing PR55 $\alpha$  protein stability. Functional tests indicate that ectopic p53<sup>R175H</sup> or PR55 $\alpha$  expression results in an increase of c-Myc protein stability with concomitant dephosphorylation of c-Myc-T58, which is a PR55 $\alpha$  substrate, whose phosphorylation otherwise promotes c-Myc degradation. A significant increase in anchorage-independent proliferation is also observed in normal human pancreatic cells expressing p53<sup>R175H</sup> or, to a greater extent, overexpressing PR55 $\alpha$ . Consistent with the common loss of p53 function in pancreatic cancer, FBXL20 mRNA expression is significantly lower in pancreatic cancer tissues compared to pancreatic normal tissues and low FBXL20 levels correlate with poor patient survival. Collectively, these studies delineate a novel mechanism by which the p53/FBXL20 axis negatively regulates PR55 $\alpha$  protein stability.

*Neoplasia* (2021) 23, 1192–1203

**Keywords:** p53, FBXL20, PR55 $\alpha$ , PP2A, c-Myc

**Abbreviations:** ATCC, American Type Culture Collection; CHX, cycloheximide; DMEM, Dulbecco's modified Eagle's medium; DMSO, Dimethyl sulfoxide; Dox, Doxycycline; esiRNAs, endoribonuclease-prepared siRNAs; FBXL20, F-Box and Leucine-Rich Repeat Protein 20; HPNE, human normal pancreatic cells; HPV16, human papillomavirus 16; IB, immunoblotting; IHC, immunohistochemistry; IP, immunoprecipitation; KSR, Kinase Suppressor of Ras 1; LATS, Large Tumor Suppressor Kinase; PP2A, protein phosphatase 2A; RT-PCR, Reverse Transcription Polymerase Chain Reaction; SCF, Skp1\_Cullin1\_F-box; siRNA, short interfering RNA; shRNA, short hairpin RNA; wt, wild-type; YAP, Yes-associated protein.

\* Corresponding author at: Department of Radiation Oncology, University of Nebraska Medical Center, 986850, Omaha, NE 68198-6805, USA.

E-mail address: [yyan@unmc.edu](mailto:yyan@unmc.edu) (Y. Yan).

Received 20 July 2021; received in revised form 2 October 2021; accepted 13 October 2021

© 2021 The Authors. Published by Elsevier Inc. This is an open access article under the CC BY-NC-ND license (<http://creativecommons.org/licenses/by-nc-nd/4.0/>) <https://doi.org/10.1016/j.neo.2021.10.002>

## Introduction

PP2A (protein phosphatase 2A) is a family of holoenzyme complexes accounting for the majority of serine/threonine phosphatase activities in human cells [1,2]. Each PP2A complex consists of one catalytic subunit, one scaffolding subunit, and one regulatory subunit [1,2]. While the scaffolding and catalytic subunits each contain only two highly conserved isoforms ( $\alpha$  or  $\beta$ ), the regulatory subunits are 26 members encoded by 15 genes and classified into four distinct subfamilies (B, B', B'' and B'''), which determine the substrate specificities of their associated PP2A complexes [1,3]. PP2A complexes serve essential roles in fundamental cellular functions, including proliferation, survival, and differentiation [1,4–7]. Thus, dysregulated PP2A activities are associated with various human diseases including autoimmune diseases and cancer [8]. PR55 $\alpha$  is a regulatory subunit of PP2A that has been shown to facilitate several oncogenic signaling pathways essential for tumorigenesis, progression, and/or metastasis of cancer [9–11]. These studies show that PR55 $\alpha$ -controlled PP2A complex (PR55 $\alpha$ /PP2A) promotes activation of the Raf/MEK/ERK oncogenic cascade through dephosphorylating their inhibitory sites KSR-S392 and Raf-S259/S295 and stabilizes  $\beta$ -catenin and c-Myc oncoproteins by dephosphorylating the  $\beta$ -catenin-T41/S37/S33 and c-Myc-T58 residues, respectively [12–16]. Furthermore, our recent studies have revealed an essential role of PR55 $\alpha$  in the activation of YAP oncogenic signaling that is required for anchorage-independent growth, cancer stem cell maintenance, and metastasis of most solid tumors. Our results also show that this role of PR55 $\alpha$ /PP2A involves its direct dephosphorylation of MOB1-T35 and LATS1/2-S909, resulting in the inhibition of the Hippo tumor suppressor pathway that negatively regulates YAP's nuclear retention and protein stability [17]. Consistent with the roles of PR55 $\alpha$  in promoting oncogenic pathways, our studies show that PR55 $\alpha$  is overexpressed in pancreatic cancer cells/tissues and required for tumorigenicity and metastasis of pancreatic cancer [15].

The p53 tumor suppressor detects genotoxic stress and coordinates diverse responding mechanisms to maintain genomic integrity and block malignant transformation [18]. Thus, over 50% of human cancers carry loss of function mutations in the p53 gene [18]. The loss of p53 function is detected in more than 80% of pancreatic cancers and serves as the main driver of pancreatic cancer [19,20]. Furthermore, the loss of p53 function is required for pancreatic cancer to progress into invasive and metastatic diseases [19,21,22]. p53 elicits its tumor suppressor function mainly by inducing the DNA-damage response that leads to cell cycle arrest and DNA repair, or apoptosis if the damage is unrepairable [20,23]. In response to DNA damage, p53 has been shown to activate VPS34, a class III phosphoinositide 3-kinase that inhibits autophagy, which, in turn, promotes the transcription of FBXL20, an F-box protein that serves as a substrate recognition component of the SCF (Skp1\_Cul1\_F-box) E3 ubiquitin ligase complexes that promote proteasomal degradation [23–25]. Previous studies have also identified PR55 $\alpha$  in promoting autophagic survival [26,27], suggesting a functional relationship of PR55 $\alpha$  and p53 in DNA damage response. On the other hand, PR55 $\alpha$  is shown to interact directly with FBXL16, which is another member of the F-box family [23,24,28]. In this study, we investigated the mechanism that regulates PR55 $\alpha$  protein expression and identified the p53/FBXL20 axis as a negative regulator of the protein stability of PR55 $\alpha$ .

## Materials and methods

### Cell culture and treatment

HPNE is a line of primary human pancreatic cells immortalized by human telomerase hTERT [29]. HPNE-E6, HPNE-E7, and HPNE-E6/E7 cell lines were established by transducing HPNE cells with retroviral vectors expressing the E6 and/or E7 proteins of HPV 16 virus [30]. HPNE/p53<sup>R175H</sup> stable clones were established by transducing HPNE cells with a lentiviral

vector, pLenti6/V5\_p53/R175H (Addgene, Watertown, MA), expressing V5-tagged p53<sup>R175H</sup> and selected with blasticidin at 4  $\mu$ g/ml (Thermo Fisher Scientific, Waltham, MA). HPNE/PR55 $\alpha$  cell line expresses Doxycycline (Dox)-inducible PR55 $\alpha$  cDNA, which was established by transducing HPNE cells with the pRevTet-On retroviral vector and selected with hygromycin at 200  $\mu$ g/ml (Clontech) expressing PR55 $\alpha$  cDNA, as described in our previous publication [17]. The panel of HPNE cell lines was maintained in Medium-D growth medium [3 parts high glucose Dulbecco's modified Eagle's medium (DMEM) (GE Healthcare Life Sciences, Pittsburgh, PA) to one-part M3:Base A (INCELL, San Antonio, TX) supplemented with 10% Tet-free FBS with 10ng/mL EGF (Invitrogen)] [29]. Ectopic PR55 $\alpha$  overexpression in HPNE/PR55 $\alpha$  cells was induced with 1 $\mu$ g/ml Dox for 48–72 h.

Human pancreatic cancer cell lines CD18/HPAF, Capan-1, BxPC-3, T3M-4, and AsPC-1 were obtained from ATCC (Manassas, VA). The Balb/c mouse cell lines were a gift from Dr. Arnold J. Levine (Institute for Advanced Study). Balb/c 3T3 (p53-wt) is a spontaneously immortal line derived from Balb/c mouse embryo fibroblasts and expresses wild-type p53. The Balb/c 3T3 (p53<sup>-/-</sup>) cell line is a derivative of Balb/c 3T3 cells that produce a p53 transcript with a stop codon at amino acid 173 and does not express a detectable level of p53 [31]. The Balb/c 3T3 (175.1) cell line was derived from the Balb/c 3T3 (p53<sup>-/-</sup>) line by stable transfection of the cells with a dominant-negative p53 mutant containing histidine to arginine substitution at codon 175 [32]. Both the Balb/c and pancreatic cancer cell lines were maintained in DMEM with 10% fetal bovine serum (FBS) in an atmosphere containing 5% CO<sub>2</sub>. Proteasome inhibitor MG132 (EMD Biosciences) was dissolved in DMSO and the cells were treated with MG132 at 10  $\mu$ M [33,34].

### Antibodies

All antibodies were purchased from Cell Signaling Technology (Danvers, MA) unless otherwise indicated. These include mouse IgG for  $\alpha$ -tubulin (DM1A), V5-Tag (E9H8O), GAPDH (6C5) (Santa Cruz Biotechnology, Santa Cruz, CA), PP2A-C subunit (1D6, EMD Millipore, Burlington, MA), PR55 $\alpha$  (2G9, EMD Millipore), p53 (DO1, Santa Cruz Biotechnology), FBXL20 (D-4, Santa Cruz Biotechnology), Ubiquitin antibody (P4D1, Santa Cruz Biotechnology), c-Myc (phospho-S62) (33A12E10, Abcam, Cambridge, UK); rabbit IgG for Ki67 (ab16667, Abcam), p53 (FL-393), PP2A-PR55 $\alpha$  Subunit [(100C1) and (#4953)], c-Myc (D3N8F), c-Myc (phospho-T58, ab85380), FBXL20 (SCRAPPER) (ProSci, Poway, CA), FBXL16 Antibody (ProSci). Secondary antibodies for immunofluorescence studies included Alexa Fluor 594 Donkey Anti-rabbit IgG and Alexa Fluor 488 Donkey Anti-mouse IgG from Thermo Fisher Scientific. Nuclei were visualized by DAPI (Sigma-Aldrich, St. Louis, MO).

### Immunoblotting, immunoprecipitation, and protein half-life analysis

Immunoblotting (IB) and immunoprecipitation (IP) were performed as described previously [15,35,36]. For the co-IP studies, PR55 $\alpha$  and FBXL20 were immunoprecipitated from 0.6–1 mg protein from the lysates of HPNE cells using anti-PR55 $\alpha$  and anti-FBXL20 rabbit antibodies, respectively, and the precipitates were probed for the presence of both PR55 $\alpha$  and FBXL20 by immunoblotting with anti-PR55 $\alpha$  and anti-FBXL20 mouse antibodies. PR55 $\alpha$  and FBXL20 in the cell lysate were measured by immunoblotting as protein loading controls. For analyzing PR55 $\alpha$  ubiquitination, PR55 $\alpha$  immunoprecipitated from 0.6–1 mg protein lysates were analyzed for PR55 $\alpha$  and ubiquitin by Western blot analysis.

To analyze protein half-life, cells were incubated with protein synthesis inhibitor cycloheximide (CHX, dissolved in water) (Sigma-Aldrich) at 15  $\mu$ g/ml for the indicated times and analyzed for specific protein expression by immunoblotting, as described in our previous study [37]. Specific proteins and loading control (GAPDH or  $\alpha$ -Tubulin) on Western blots were

visualized by chemiluminescence exposed to x-ray films, scanned using an EPSON Perfection 4490PHOTO scanner, and quantified with Fiji-ImageJ analytical program (NIH, Bethesda, MD). The levels of specific proteins were normalized with the control protein levels and calculated for half-life times  $[t(1/2)]$  by linear regression analysis of log (protein level) against time using the SigmaPlot graphing and data analysis software, as described in our studies [38].

### Short interfering RNAs and transfection

The ON-TARGETplus SMARTpool of siRNA duplexes (Dharmacon, Lafayette, CO) for silencing FBXL20 contains four siRNAs targeting multiple sites on the FBXL20 mRNA. The sequences of FBXL20 siRNAs are 5'-GCCUGAGCUAGUGACUUU-3', 5'-GGAUGGCAU UCAAGCACUA-3', 5'-GGUGUGACCAAGUAACCAA-3', and 5'-UACCAUAUGCAGAGGGUGU-3'. For validation, FBXL20 was also knocked down with endoribonuclease-prepared siRNAs (esiRNAs) targeting a region of FBXL20-mRNA (EMU193711, Millipore-Sigma). The sequence for generating the FBXL20 esiRNAs is 5'-CCTGCACTAGCCTTA GCAAGTTCTGCTCCAAACTCAGACACCTCGACTTGGCTTCCTG TACGTCAATAACAAACATGTCTCTAAAAGCTCTGAGTGAGGGCT GTCCACTGTTGGAGCAGTTGAACATTTCTGGTGTGACCAAGT AACCAAGGATGGCATTCAAGCACTAGTGAGAGGCTGTGGGGGT CTCAAGGCCCTTATTCTTAAAAGGCTGCACTCAGCTAGAAGATGA AGCTCTCAAGTACATAGGTGCACACTGCCCTGAGCTAGTGACTT TAAACCTGCAAACCTTGCTTACAAATCACAGATGAAGGTCTCATT A CCATATGCAGAGGGGTGCATAAGTTGCAGTCCCTCTGTGCCTCT GGGTGCTCCAATATCACAGATGCCATCCTGAACGCTCTAGGTCA GAAGTGGCC-3'. The sequences of the SMART siRNAs pool silencing p53 are 5'-GAAAUUUGCGUGUGGAGUA-3', 5'-GUGCAGCUGU GGUUGAUU-3', 5'-GCAGUCAGAUCCUAGCGUC-3', and 5'-GGAGAAUUAUUCACCCUUC-3'. The sequence of the control siRNA is 5'-UAGCGACUAAACACAUCAA-3'.

Cells were transfected with 100 pmol of siRNA and incubated for 48–72h before analysis. All cell lines were transfected with DharmaFECT-1 (Thermo Fisher Scientific) as instructed by the manufacturer.

The sequences of shRNAs targeting the human PR55 $\alpha$  (PPP2R2A) mRNA are 5'-ATGGCTAGCAGACATGGAG-3', and 5'-CAACTATCTCAACTAAGCA-3' and the sequence for the non-silencing Control-shRNA is 5' ATCTCGCTTGGGCGAGAGTAAAG-3' (Dharmacon). Transduction of CD18/HPAF cells with Control-shRNA and PR55 $\alpha$ -shRNAs were done as described in our publication [17].

### Immunofluorescence and microscopy

Immunofluorescence and microscopy were performed as described previously [17,35]. Briefly, cells grown on coverslips (#1-thickness) were fixed in 4% paraformaldehyde (PFA) for 20 min, followed by incubation with 0.25% Triton X-100 for 10 min to achieve permeabilization. Samples were then blocked for 30 min using 10% horse serum, 1% bovine serum albumin (BSA), and 0.5% Tween-20 in TBS at ambient temperature. To analyze the co-localization of PR55 $\alpha$  with FBXL20, cells were incubated overnight at 4°C in anti-FBXL20 (SCRAPPER) rabbit IgG (1:50 dilution) and anti-PR55 $\alpha$  mouse IgG (2G9) (1:200 dilution) in TBS/0.05% Tween-20. After washing with 1% BSA in TBS, cells were incubated with Alexa Fluor 594 anti-rabbit IgG (1:200 dilution, Cat. #A-21207) and Alexa Fluor 488 anti-mouse IgG, (1:200 dilution, Cat. #A-21202) for 1 hr in dark. DAPI staining occurred at a 1:1000 dilution for 5 min. Images were taken with a Zeiss-810 confocal laser-scanning microscope. FBXL20 and PR55 $\alpha$  in the nuclei and cytoplasm, as well as their co-localization, were analyzed by Fiji-ImageJ [39–41].

### Spheroid culture in soft-agar and immunohistochemistry analysis

As described previously in our studies [17,42], cells were plated at 50k cells/well in 6-well plates in Medium-D growth medium containing 0.35% NuSieve Agarose Soft-agar (FMC Bioproducts, Rockland, ME) and cultured for 3–6 weeks. The medium for HPNE/PR55 $\alpha$  cells contained Dox (1 $\mu$ g/ml) for maintaining ectopic PR55 $\alpha$  expression. The Spheroids were collected using cell strainers (Corning, Tewksbury, MA) by centrifugation at 2000-RPM for 2 min, washed with PBS, and fixed in 4% PFA overnight at 4°C. Following fixation, Spheroids were washed with PBS, incubated in 30% sucrose solution for 24–48 h at 4°C, embedded into Histogel (ThermoFisher, Waltham, MA), and analyzed for Ki67 proliferation marker with ab16667 at 1:200 dilution by immunohistochemistry (IHC) and Hematoxylin Counter Staining as described by the manufacturer. IHC analysis of FBXL20 expression in human pancreatic ductal adenocarcinoma tissue was carried out with the FBXL20 (SCRAPPER) rabbit IgG at 1:400 dilution, as described by the previous studies [15].

### RT-PCR analysis

As described in our previous study [17], total RNA was isolated from the indicated cells using the TRIzol RNA-Isolation Reagent (Invitrogen) and analyzed for human PR55 $\alpha$  and GAPDH mRNA levels by real-time RT-PCR using the iScript Advanced cDNA Synthesis Kit (Quanta Biosciences) and SsoAdvanced Universal SYBR Green Supermix (Bio-Rad). The PR55 $\alpha$  mRNA expression was normalized with GAPDH mRNA levels. The PCR primer sequences for human GAPDH include forward-primer 5'-CCACTCCTCCACCTTTGA-3', and Reverse-primer 5'-ACCCTGTTGCTGTAGCCA-3'. The PCR primer sequences for human PR55 $\alpha$  (gene name PPP2R2A) include forward-primer 5'-GCAACAGGAGATAAAGGTGGTAG-3' and reverse-primer 5'TGGTTCATGGCTCTGGAAGGTG-3'. The PCR primer sequences for mouse GAPDH include forward-primer 5'-TTCCACCCATGGCAAATT-3', and reverse-primer 5'-TGGCAGGTTTTTCTAGAC-3'. The PCR primer sequences for mouse PPP2R2A include forward-primer 5'-GAGACAAAAGACCAGAAGGCTATA-3' and reverse-primer 5'-ATTCTCCGTGGACTGGCTTCCA-3'.

### Statistical analysis

Student's t-test and one-way ANOVA methods were used for the comparison of experimental groups using SigmaPlot software. Linear regression analysis of log (protein level) against time was used to calculate protein half-life (Figs. 2, 3D,E, and 6D) with SigmaPlot software. The Kaplan-Meier method was used to assess the correlation between FBXL20 mRNA expression and the survival of pancreatic cancer patients (Fig. 7C) using GraphPad Prism-8 software. For all the statistical analyses, *P* values  $\leq 0.05$  were considered significant.

## Results

### Inactivation of p53 function increases the stability of PR55 $\alpha$ protein

We tested the effect of p53 function on PR55 $\alpha$  protein expression in human normal pancreatic cells (HPNE), which were immortalized by human telomerase, and mouse embryonic Balb/c 3T3 cells. In HPNE cells, PR55 $\alpha$  protein expression was always higher in the cells engineered to lack wild-type (wt) p53 function, either by siRNA-knockdown, expressing the viral oncoprotein HPV16-E6 that promotes p53 degradation [43] or expressing the dominant-negative mutant p53 (p53<sup>R175H</sup>) (Fig. 1A–C). In contrast, ectopically expressing HPV16-E7, which promotes the degradation of the pRB tumor suppressor [44], had little effect on PR55 $\alpha$  protein level in HPNE

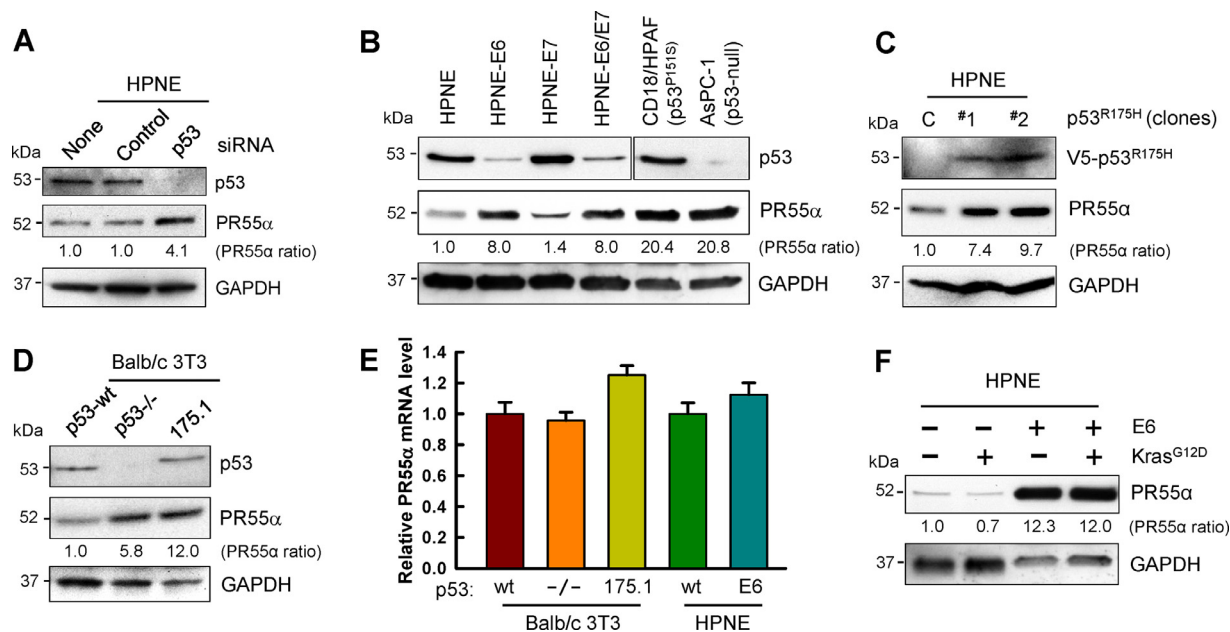


**Fig. 1.** Loss of p53 suppressor function increases the PR55 $\alpha$  protein level. (A-C) In the HPNE human pancreatic normal cells, loss of wild-type (wt) p53 function was produced by siRNA transfection (A), expressing HPV16-E6 that induces p53 degradation (HPNE-E6) (B), or expressing p53<sup>R175H</sup>, a loss-of-function of mutant p53 (C). The cell lysates were analyzed for protein expression of p53, PR55 $\alpha$ , and GAPDH by immunoblotting. As a positive control, pancreatic cancer cell lines CD18/HPAF and AsPC-1, which express p53<sup>P151S</sup> mutant and p53-null (resulted by p53 frame-shift/TGC→GC), respectively, were included in the analysis. The densities of PR55 $\alpha$  and GAPDH signals on the blots were quantified by Fiji-ImageJ software, and relative PR55 $\alpha$  levels were determined after normalization by GAPDH levels. Note: Fig. 1B, p53 panels were from the same x-ray film. (D) In mouse Balb/c 3T3 cells, loss of wt-p53 function was produced by expressing p53<sup>R175H</sup> or homologous p53 deletion (p53<sup>-/-</sup>). The effects of these interventions on PR55 $\alpha$  protein expression were determined by Western blot analysis. Relative PR55 $\alpha$  levels in the samples were determined as described above. (E) p53-proficient (wt) and -deficient HPNE (human) and Balb/c 3T3 (mouse) cells were analyzed and compared by RT-PCR for PR55 $\alpha$ -mRNA levels, which show no significant differences among the samples. (F) The oncogenic Kras<sup>G12D</sup> mutant does not affect PR55 $\alpha$  protein expression. HPNE-Control and HPNE-E6 cells were stably transduced with mutant Kras<sup>G12D</sup> with a retroviral vector and analyzed for PR55 $\alpha$  protein expression by immunoblotting. Relative PR55 $\alpha$  levels in the samples were determined as described above.

cells (Fig. 1B). As a positive control, the analysis included two pancreatic cancer cell lines that lack p53 function [45], CD18/HPAF expressing the p53<sup>P151S</sup> mutant, and AsPC-1 harboring p53 frame-shift/TGC→GC resulting in p53-null, both of which showed overexpression of PR55 $\alpha$  (Fig. 1B). Consistently, mouse Balb/c 3T3 cells engineered to lack wt-p53 function either by p53 deletion (p53<sup>-/-</sup>) or expressing the p53<sup>R175H</sup> mutant also exhibited increased PR55 $\alpha$  protein levels (Fig. 1D). Furthermore, RT-PCR analysis showed no significant difference in PR55 $\alpha$  mRNA level among the cell lines, irrespective of p53 status (Fig. 1E), suggesting that the regulation of PR55 $\alpha$  by p53 occurs at the protein level. As a comparison, we examined the effect of oncogenic mutant Kras<sup>G12D</sup> expression on PR55 $\alpha$ -protein expression in HPNE cells. As shown in Fig. 1F, while expressing HPV16-E6 markedly increased PR55 $\alpha$ -protein level in HPNE cells, expressing the Kras<sup>G12D</sup> mutant had little effect on PR55 $\alpha$ -protein levels in the cells.

Subsequently, we tested the effect of proteasome inhibition by MG132 on PR55 $\alpha$  protein expression. As shown in Fig. 2A, MG132 treatment resulted in ~4-fold increase in the level of PR55 $\alpha$  protein in p53-proficient HPNE or Balb/c 3T3 cells (p53-wt), whereas it did not affect the already high PR55 $\alpha$  level in p53-deficient HPNE or Balb/c 3T3 cells (HPV-E6, p53<sup>-/-</sup> or p53<sup>R175H</sup>). We then measured PR55 $\alpha$  protein stability in the isogenic HPNE and Balb/c 3T3 cell lines, which differ only in p53 function, using the CHX-chase assay as described in our previous study [17]. The results showed that loss of p53 function in human HPNE cells or mouse Balb/c 3T3 cells resulted in a marked extension of PR55 $\alpha$  protein half-life (Fig. 2B,C).

*p53-supported FBXL20 negatively regulates the protein-stability of PR55 $\alpha$*

Previous studies show that FBXL20 is transcriptionally induced by p53 as part of the DNA damage response, while FBXL16 is shown to bind directly to PR55 $\alpha$  [23–25,28]. Therefore, we compared the effect of p53 function on the protein expression of FBXL16 and FBXL20, both of which are F-box family members serving as the adapters on the SCF E3 ubiquitin ligase complexes [24]. As shown in Fig. 3A,B, inactivation of p53 function by expressing the p53<sup>R175H</sup> mutant, p53 homologous deletion (p53<sup>-/-</sup>), or siRNA-knockdown led to marked decreases in FBXL20 protein expression in both human and mouse cells. In contrast, the same interventions did not result in a decrease in FBXL16 protein level.

Next, we examined the effect of FBXL20 on PR55 $\alpha$  expression with siRNAs. As shown in Fig. 3C, transfection with FBXL20-siRNA significantly reduced the FBXL20 protein level in HPNE/Control cells, which express wild-type p53, and resulted in an approximately 10-fold increase in PR55 $\alpha$  protein level. In contrast, transfection of FBXL20-siRNA had little effect on the already low FBXL20 level in HPNE/p53<sup>R175H</sup> cells, as well as on the high PR55 $\alpha$  level in these cells. Furthermore, there was very little difference in the PR55 $\alpha$  level between the HPNE/Control cells transfected with FBXL20-siRNAs and the HPNE/p53<sup>R175H</sup> cells transfected with/without FBXL20-siRNA (lane 2 vs. lanes 3-5).

Subsequently, we assessed the effect of FBXL20 on PR55 $\alpha$  protein stability using the CHX-chase method [17]. The result showed that FBXL20-

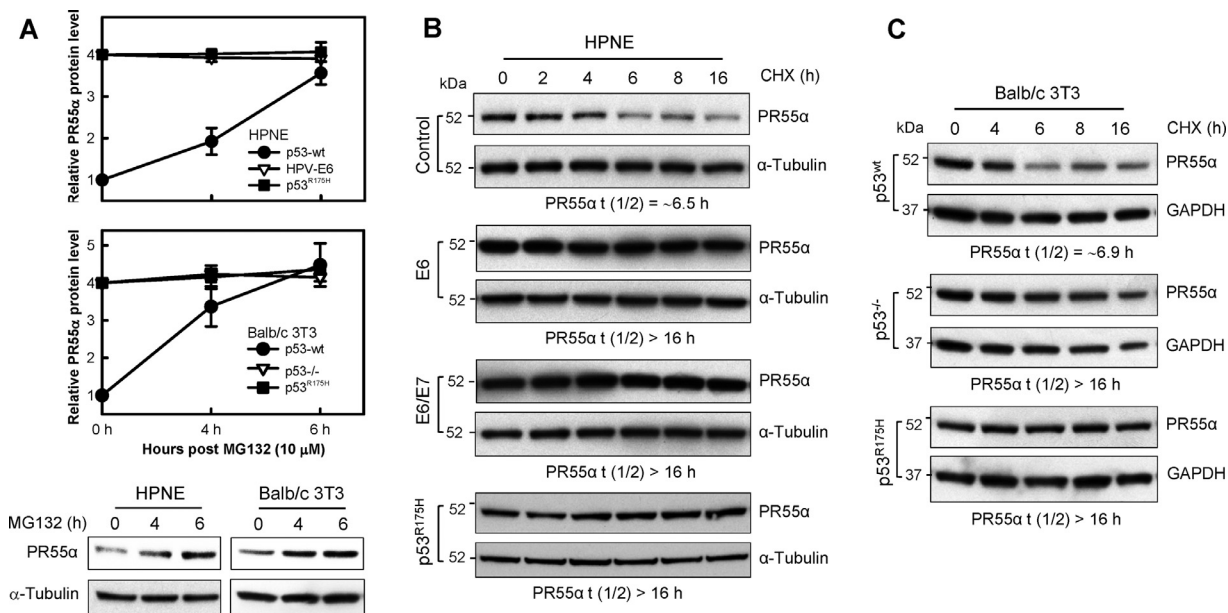


**Fig. 2.** Loss of p53 function increases PR55 $\alpha$  protein stability. (A) Inhibition of the proteasome by MG132 only increases PR55 $\alpha$  protein level in p53-wt cells. HPNE and Balb/c 3T3 cells proficient (p53-wt) or deficient in p53 function (HPV-E6, p53<sup>R175H</sup>, or p53<sup>-/-</sup>) were incubated in the media containing proteasome inhibitor MG132 (10  $\mu$ M) for 0, 4, and 6 h, and followed by Western blot analysis for the levels of PR55 $\alpha$  and  $\alpha$ -Tubulin (loading control). Line-graphs: PR55 $\alpha$  and  $\alpha$ -Tubulin signals captured by x-ray films were quantified by Fiji-ImageJ software, and relative PR55 $\alpha$  levels at the indicated time points were determined after normalization by  $\alpha$ -Tubulin levels. The experiment was repeated three times and the results were expressed as mean $\pm$ S.D. (n=3). Bottom panel: Representative Western blot analyses of PR55 $\alpha$  and  $\alpha$ -Tubulin (loading control) in HPNE and Balb/c 3T3 control cells following treatment with MG132 for the times indicated. (B-C) Assessment of PR55 $\alpha$  protein half-life using the cycloheximide-chase assay. As described in *Materials and Methods* [17], the HPNE and Balb/c 3T3 isogenic cell panels differed only in p53 function were treated with 15  $\mu$ g/ml cycloheximide (CHX) for the indicated hours and analyzed for the protein levels of PR55 $\alpha$  and  $\alpha$ -Tubulin or GAPDH by immunoblotting. The signals on the blots were quantified by Fiji-ImageJ software, and relative PR55 $\alpha$  levels were determined after normalization by  $\alpha$ -Tubulin or GAPDH levels. Protein half-life  $t(1/2)$  of PR55 $\alpha$  was calculated by linear regression analysis of log (PR55 $\alpha$  level) against time using SigmaPlot software. The values shown represent the average of two independent experiments.

knockdown by siRNAs extended PR55 $\alpha$  protein half-life from ~6 h to ~12 h in both HPNE and Balb/c 3T3 cells (Fig. 3D,E). For validation, FBXL20 was also knocked down using esiRNAs (EMU193711, Millipore-Sigma), as described in *Materials and Methods* [46], and similar results were obtained (data not shown).

#### Loss of p53 function or FBXL20 expression reduces PR55 $\alpha$ -ubiquitination

We analyzed the effect of p53 function on PR55 $\alpha$ -ubiquitination in HPNE and Balb/c 3T3 cells. The cells with/without p53 function were incubated with MG132 (10  $\mu$ M) or 0.1% DMSO (vehicle control) for 6 h to block protein degradation, immunoprecipitated (IP) with anti-PR55 $\alpha$  antibody, and analyzed for PR55 $\alpha$ -ubiquitination by immunoblotting (IB), as described previously [35]. As shown in Fig. 4A (top panel), the level of PR55 $\alpha$ -ubiquitination reduced by 83% in HPNE/p53<sup>R175H</sup> cells compared to HPNE/Control (p53<sup>wt</sup>) cells. The detection was specific, as PR55 $\alpha$ -ubiquitination was not present in HPNE/Control cells without inhibition of proteasome activity by MG132 (Fig. 4A, top panel, lane 1). Similarly, the level of PR55 $\alpha$ -ubiquitination was reduced by 87% in Balb/c 3T3 (p53<sup>-/-</sup>) cells relative to Balb/c 3T3 (p53<sup>wt</sup>) cells (Fig. 4A, bottom panel).

Next, we examined the effect of FBXL20 expression on PR55 $\alpha$ -ubiquitination. For this study, HPNE and Balb/c cells were transfected with FBXL20-siRNAs for 3 days and treated with MG132 for 6h before analyzing PR55 $\alpha$  ubiquitination. As shown in Fig. 4B, FBXL20-knockdown resulted

in the diminution of PR55 $\alpha$ -ubiquitination by 77% and 80% in HPNE and Balb/c 3T3 cells, respectively.

Together, the results in Figs. 3,4 show that either loss of p53 function or decrease of FBXL20 expression diminishes PR55 $\alpha$ -ubiquitination. This is linked to an increase in PR55 $\alpha$  protein stability. Thus, this data suggests a role of p53/FBXL20 cascade in the promotion of PR55 $\alpha$  proteasomal degradation.

#### FBXL20 interacts with PR55 $\alpha$ in vitro and in vivo

We tested the interaction of PR55 $\alpha$  and FBXL20 in HPNE cells by reciprocal co-immunoprecipitation (IP), as described previously in our study [17]. Immunoblotting (IB) revealed the presence of both PR55 $\alpha$  and FBXL20 in the immunoprecipitates obtained from HPNE lysates with either anti-PR55 $\alpha$  or anti-FBXL20 antibody (Fig. 5A), while neither were detected in the control immunoprecipitates obtained with non-immunized IgG.

Next, we analyzed the intracellular co-localization of PR55 $\alpha$  and FBXL20 in HPNE cells by immunofluorescence (IF) confocal microscopy, as described in our studies [17,35]. The results in Fig. 5B-D (HPNE/Control) showed that PR55 $\alpha$  and FBXL20 were present in both the cytoplasm and nucleus of the cells, with PR55 $\alpha$  expression relatively higher in the nucleus. When ectopic PR55 $\alpha$  expression was induced by Dox (1 $\mu$ g/ml) in HPNE cells (HPNE/PR55 $\alpha$ ), the nuclear-portion of PR55 $\alpha$  was significantly augmented ( $P=0.004$ ) (Fig. 5B-C). A simultaneous increase in the nuclear portion of FBXL20 was also detected in the HPNE/PR55 $\alpha$ , although

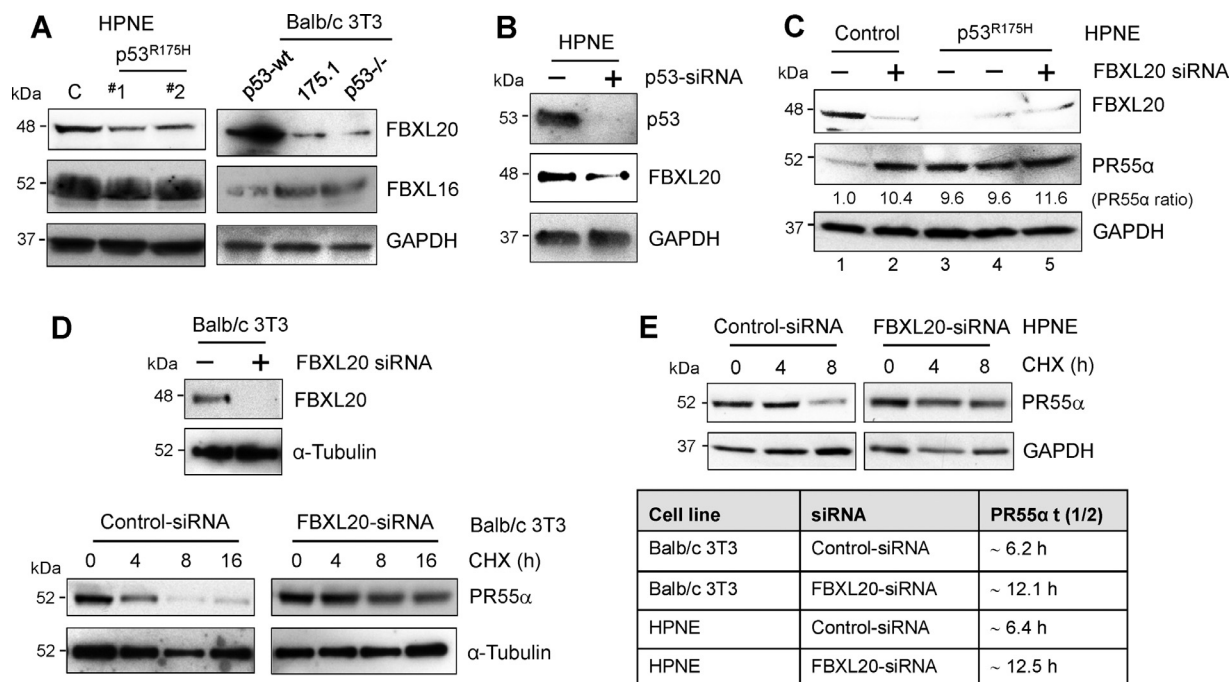


**Fig. 3.** FBXL20 is required for p53 to suppress PR55 $\alpha$  protein stability. (A) Effect of p53 function on FBXL20 expression. Left panel: Human HPNE cells stably transduced with control vector (C) or p53<sup>R175H</sup> (clones #1 and #2) were analyzed for FBXL20, FBXL16, and GAPDH protein levels by Western blotting. Right panel: Balb/c 3T3 mouse cells expressing p53-wt, p53-R175H (175.1), and p53<sup>-/-</sup> were analyzed for FBXL20, FBXL16, and GAPDH protein levels by Western blotting. (B) HPNE cells were transfected with p53-siRNAs for 3 days and analyzed for the indicated proteins by Western blotting. (C) Effect of FBXL20 on PR55 $\alpha$  protein expression. HPNE cells were transfected with Control-siRNAs or FBXL20-siRNAs for 72 h and analyzed for FBXL20, PR55 $\alpha$ , and GAPDH by Western blotting. (D) Effect of FBXL-20 on PR55 $\alpha$  protein stability. Top panel: Balb/c 3T3 mouse cells were transfected with Control-siRNAs or FBXL20-siRNAs for 72 h and analyzed for FBXL20 and  $\alpha$ -Tubulin levels by immunoblotting. Bottom panel: following siRNA-transfection for 72 h, the cells were incubated in the medium containing CHX (15  $\mu$ g/ml) to halt protein synthesis for 0, 4, 8, 16, and 24 h and analyzed for PR55 $\alpha$  and  $\alpha$ -Tubulin protein levels by Western blotting. (E) Top panel: HPNE cells were transfected with Control-siRNAs or FBXL20-siRNAs for 72 h, incubated in the medium containing CHX (15  $\mu$ g/ml) for the indicated hours, and analyzed for PR55 $\alpha$  and GAPDH protein levels. Table: the density of PR55 $\alpha$  signals in Fig. 3D (bottom panel) and Fig. 3E (top panel) were quantified by Fiji-ImageJ software, normalized with  $\alpha$ -Tubulin (Fig. 3D) and GAPDH (Fig. 3E), respectively, and analyzed for the protein half-life of PR55 $\alpha$  by linear regression analysis of log (PR55 $\alpha$  level) against time. The PR55 $\alpha$  t(1/2) values represent the average of two independent experiments.

the increase was slightly below statistical significance ( $P=0.055$ ) (Fig. 5B and D). Co-localization studies revealed that there was a significant decrease in the colocalization of PR55 $\alpha$  and FBXL20 in the PR55 $\alpha$ -high cells (HPNE/PR55 $\alpha$ ) compared to the isogenic PR55 $\alpha$ -low cells (HPNE/Control) (Fig. 5E)

*Ectopic expression of the p53<sup>R175H</sup> mutant or PR55 $\alpha$  increases the protein stability of c-Myc*

c-Myc serves as a master regulator of cellular metabolism and proliferation. Aberrant c-Myc activation stimulates numerous metabolic changes that not only promote oncogenic transformation but also support the malignant phenotypes of cancer cells [11,47,48]. The intracellular level of c-Myc is mainly regulated by its stability via the phosphorylation of its S62 and T58 sites (Fig. 6A). c-Myc is a substrate of PR55 $\alpha$ , and dephosphorylation of c-Myc-T58 by the PR55 $\alpha$ /PP2A complex prevents c-Myc proteasomal degradation, thus stabilizing c-Myc protein (Fig. 6A) [16]. Alternatively, phosphorylation of c-Myc-S62 also promotes c-Myc stabilization, which is antagonized by a different PP2A regulatory subunit, PR61 $\alpha$  [49,50] (Fig. 6A). Therefore, we examined the effects of p53<sup>R175H</sup> and PR55 $\alpha$  on c-Myc phosphorylation at these sites, as well as on c-Myc protein level and stability.

As shown in Fig. 6B, expressing ectopic p53<sup>R175H</sup> mutant or PR55 $\alpha$  in HPNE normal cells resulted in a decrease in c-Myc-T58 phosphorylation by ~84% and ~100%, respectively, as well as an induction in c-Myc protein level by 6.7-fold and 11.1-fold, respectively. For comparison, we analyzed c-Myc-S62 phosphorylation in these cells, as it also regulates c-Myc stability [16]. However, expressing either the ectopic p53<sup>R175H</sup> or PR55 $\alpha$  had little effect on c-Myc-S62 phosphorylation in HPNE cells (Fig. 6B). To verify the effect of PR55 $\alpha$  on c-Myc, PR55 $\alpha$  was knocked down by two different shRNAs in CD18/HPAF pancreatic cancer cells, which express the p53<sup>P151S</sup> mutant [51–53]. As shown in Fig. 6C, knockdown of PR55 $\alpha$  in CD18/HPAF cells resulted in induction in c-Myc-T58 phosphorylation with a concomitant decrease in total c-Myc protein levels.

Subsequently, we assessed the effects of p53<sup>R175H</sup> or PR55 $\alpha$  on c-Myc protein stability using the CHX-chase assay [17]. The results showed that ectopic expression of p53<sup>R175H</sup> mutant and PR55 $\alpha$  in HPNE cells resulted in an approximately 3-fold and 4-fold increase in c-Myc protein half-life, respectively (Fig. 6D).

We have previously demonstrated that PR55 $\alpha$  overexpression promotes anchorage-independent colony formation of HPNE cells [17]. Since p53<sup>R175H</sup> and PR55 $\alpha$  increase c-Myc stability and c-Myc promotes transformation-associated proliferation [47], we assessed the effect of p53<sup>R175H</sup> and PR55 $\alpha$  on anchorage-independent proliferation in HPNE cells. HPNE/p53<sup>R175H</sup>, HPNE/PR55 $\alpha$ , and HPNE/Control cells were

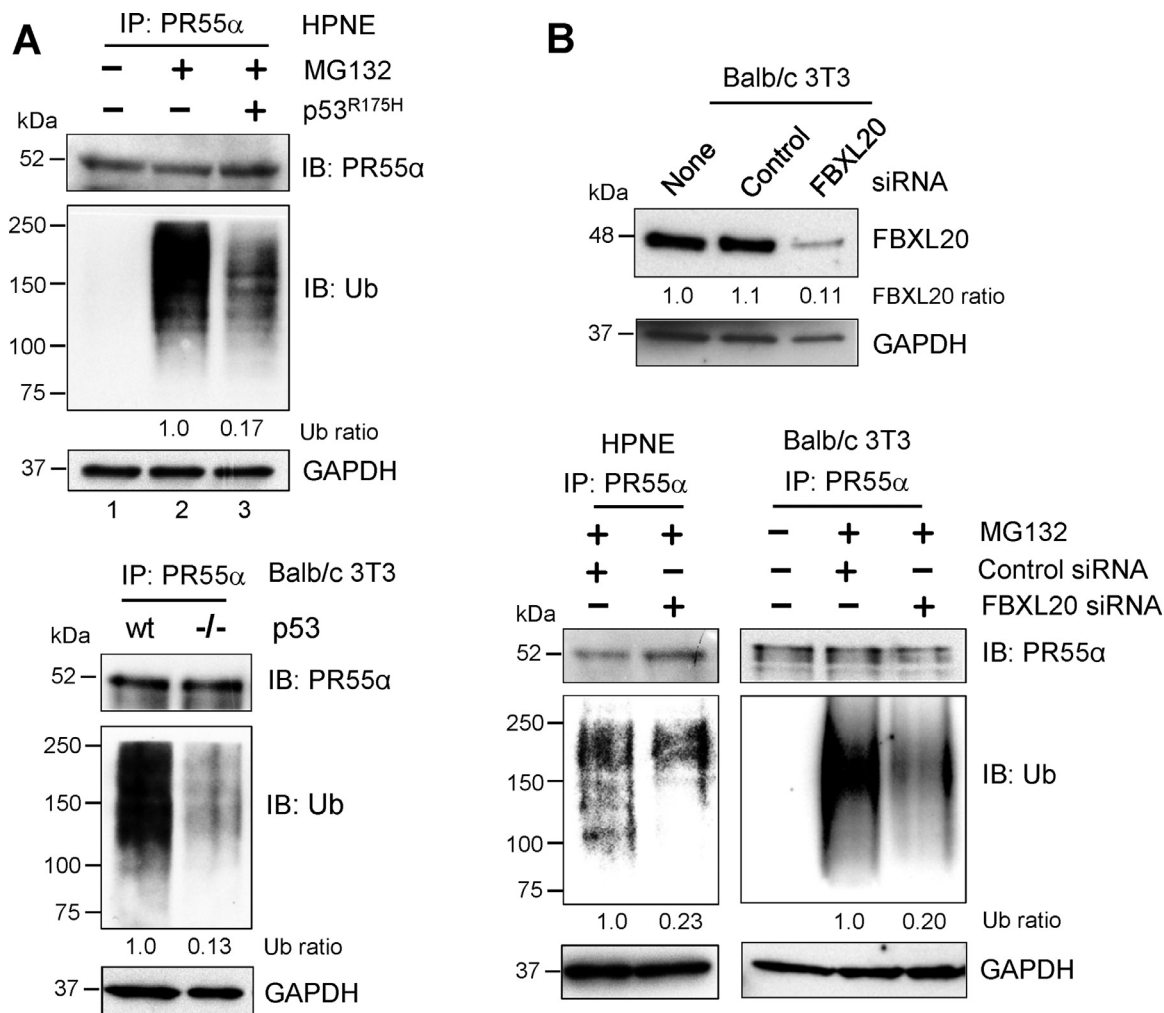


**Fig. 4.** Loss of p53 function or FBXL20 expression reduces the ubiquitination of PR55 $\alpha$ . (A) Top panel: HPNE/Control and HPNE/p53<sup>R175H</sup> cells were incubated with 10  $\mu$ M MG132 proteasome inhibitor (lanes 2-3) for 4h. As a control, HPNE/Control cells were incubated with the DMSO vehicle (lane 1). The cells were lysed, and 1 mg lysate samples were immunoprecipitated with anti-PR55 $\alpha$  (100C1) rabbit IgG (IP). The obtained immunoprecipitates were analyzed for PR55 $\alpha$  ubiquitination with anti-ubiquitin (P4D1) and anti-PR55 $\alpha$  (2G9) Mouse IgG by immunoblotting (IB). As protein loading controls, 25  $\mu$ g whole-cell lysates were assessed for GAPDH protein levels by Western blotting (*GAPDH*). The densities of ubiquitin (Ub) and GAPDH signals were quantified by Fiji-ImageJ software and determined for relative Ub levels after normalization by GAPDH levels. Bottom panel: Balb/c 3T3 cells, p53-wt and p53-/-, were incubated with 10  $\mu$ M MG132 for 4 h, and 1 mg protein lysates were analyzed for PR55 $\alpha$ -ubiquitination as described above. (B) Top panel: Balb/c 3T3 cells were transfected with none, Control-siRNAs or FBXL20-siRNAs, incubated for 72 h and analyzed for FBXL20 and GAPDH levels by Western blotting. Relative FBXL20 levels in the lysates were determined as described above. Bottom panel: indicated cells were transfected with Control-siRNAs or FBXL20-siRNAs for 72 h and then incubated with 10  $\mu$ M MG132 for 4 h. As a negative control, un-transfected Balb/c 3T3 cells incubated with the DMSO vehicle for 4 h were included in the analysis. The resulting cells were lysed, and 1 mg protein lysates were analyzed for PR55 $\alpha$ -ubiquitination as described above.

plated in soft-agar in growth medium for 3-weeks and quantified for the number of cells positive in Ki67 expression, a hallmark for cell proliferation [54]. Immunohistochemistry analysis (IHC) revealed a 4-fold and 7-fold increase in the number of Ki67-positive cells in the spheroids formed by HPNE/p53<sup>R175H</sup> and HPNE/PR55 $\alpha$  cells, respectively, compared to HPNE/Control cells (Fig. 6E).

*FBXL20 expression significantly decreases in pancreatic cancer cell lines/tissues and negatively associates with poor survival of pancreatic cancer patients*

We have previously shown that the PR55 $\alpha$  protein is overexpressed in pancreatic cancer and high levels of PR55 $\alpha$  are associated with poor patient

survival [15]. Thus, we analyzed FBXL20 protein expression in panels of pancreatic normal and cancer cell lines and tissues. As shown in Fig. 7A, FBXL20 was detected at much lower levels in the pancreatic cancer cell lines, which also express the mutant p53, as compared to HPNE normal control [51–53]. Consistently, both PR55 $\alpha$  and c-Myc protein levels were much higher in the pancreatic cancer cell lines relative to HPNE normal cells, along with much lower levels of c-Myc-T58 phosphorylation detected in the pancreatic cell lines compared to HPNE control (Fig. 7A). These results together with the data in Fig. 6 suggest an inverted functional relationship between the p53/FBXL20 axis and the PR55 $\alpha$ /c-Myc cascade. The studies also reveal a positive correction of p53 mutations with the diminution of the FBXL20 expression and with the increase in PR55 $\alpha$  and c-Myc protein levels.

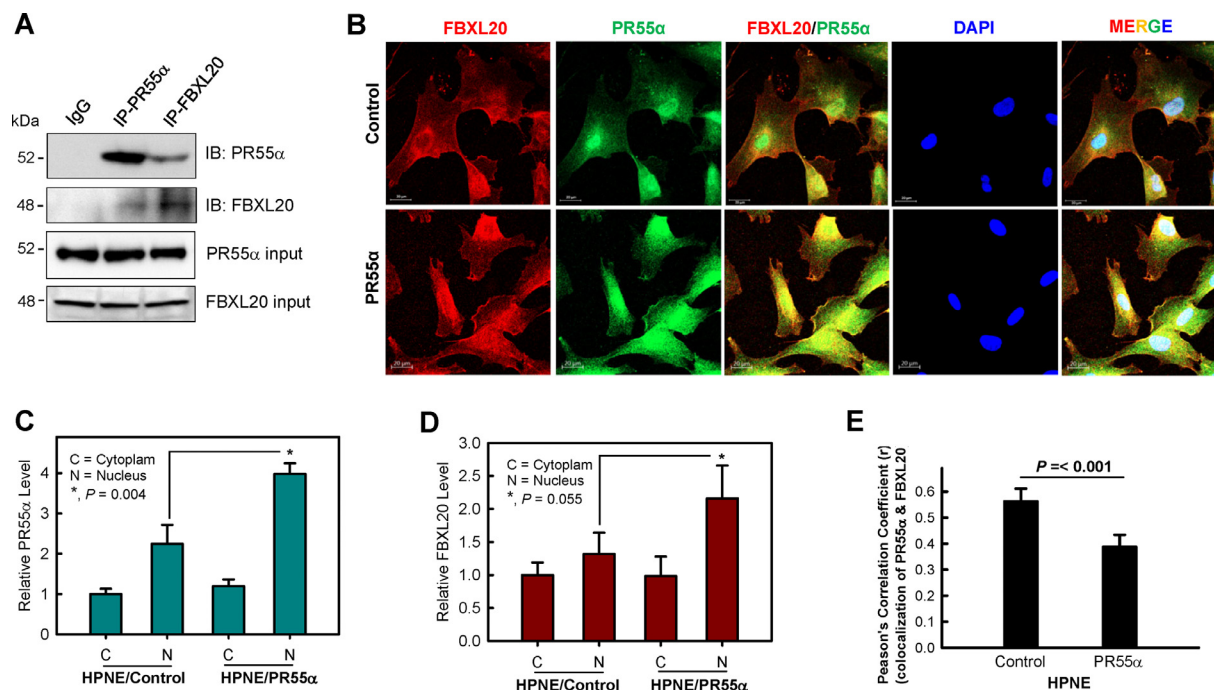


**Fig. 5.** Interaction of FBXL20 and PR55 $\alpha$  in human normal pancreatic cells. (A) PR55 $\alpha$  or FBXL-20 was immunoprecipitated (IP) from 1 mg HPNE cell lysates with the anti-PR55 $\alpha$  (100C1) (*IP-PR55 $\alpha$* ) or anti-FBXL20 (Prosci # 4449) (*IP-FBXL20*) rabbit polyclonal IgG and immunoblotted for the presence of both PR55 $\alpha$  and FBXL20 with anti-PR55 $\alpha$  (2G9) and anti-FBXL20 (D-4, SC-515274) mouse monoclonal antibody, respectively (IB). As a negative control, immunoprecipitate obtained with non-immunized rabbit IgG was included in the analysis (*IgG*). As protein loading controls, PR55 $\alpha$  and FBXL20 in the lysate were analyzed by immunoblotting (input). (B) Intracellular distribution and co-localization of FBXL20 and PR55 $\alpha$ . HPNE control (*Control*) or HPNE-transduced with Doxycycline (Dox)-inducible ectopic PR55 $\alpha$  (*PR55 $\alpha$* ) were incubated with 1  $\mu$ g/ml Dox for 2 days (to induce ectopic PR55 $\alpha$  expression) were stained with anti-FBXL20 rabbit IgG (Prosci # 4449) and anti-PR55 $\alpha$  mouse IgG (2G9). The intracellular localization of FBXL20 and PR55 $\alpha$  in the cells were analyzed using a Zeiss-810 confocal laser-scanning microscope, as described in *Materials and Methods*. Co-localization of FBXL20 and PR55 $\alpha$  in the cells were shown as merged images (*FBXL20/PR55 $\alpha$*  and *MERGE*). Scale bars, 20  $\mu$ m. (C-D) FBXL20 and PR55 $\alpha$  were analyzed for their cytoplasmic and nuclear levels using Fiji-ImageJ and SigmaPlot software with the method described previously [17]. The bar graphs show the average levels of PR55 $\alpha$  (C) and FBXL20 (D) in the cytoplasm and nuclei of  $\sim$ 120 cells measured individually. (E) The degrees of co-localization of PR55 $\alpha$  with FBXL20 in the indicated cells were measured by Fiji-ImageJ software using Pearson's overlap coefficients method and compared by Student's t-test by SigmaPlot software as described in our study [17].

Next, we analyzed FBXL20 mRNA expression in human normal and malignant pancreatic tissues from the GENT2 database (GPL570 platform) (data set: HG-U133 Plus 2) [55]. As shown in Fig. 7B and Supplementary Table S1, pancreatic cancer tissues expressed significantly lower levels of FBXL20 mRNA relative to normal pancreatic tissues ( $P = < 0.001$ ). We then analyzed the relationship of FBXL20 expression and the survival of pancreatic cancer patients with the RNA-sequencing data available from the Human Protein Atlas database [56]. The results showed that low FBXL20 mRNA levels were associated with poor survival of pancreatic cancer patients, as determined by Kaplan-Meier analysis (Fig. 7C,D and Supplementary Table S2).

In summary, the studies in this report delineate a novel mechanism by which p53 and its gene target FBXL20 negatively regulates PR55 $\alpha$  protein stability through ubiquitin-mediated proteasomal degradation. The data also reveal a positive correlation of p53 mutations with the decrease in FBXL20 expression and induction of PR55 $\alpha$  and c-Myc protein levels.

## Discussion

PR55 $\alpha$ /PP2A complex positively regulates several core oncogenic pathways including the ERK, Wnt/ $\beta$ -catenin, c-Myc, and YAP pathways [12,15,17,50,57]. Our previous studies reveal that PR55 $\alpha$  protein level

progressively increases during pancreatic cancer development and knockdown of PR55 $\alpha$  by shRNA abrogates both tumorigenicity and metastasis of pancreatic cancer cells in mouse models [15]. Since oncogenic Kras activation and loss of p53 tumor suppressor due to mutations are the key drivers of pancreatic cancer [58], we examined their effects on PR55 $\alpha$  expression in both human and mouse cells. The results of these studies delineate a novel role of p53 and its gene target FBXL20 in the negative regulation of PR55 $\alpha$  protein stability.

FBXL20 is a transcriptional target of p53 in DNA damage response [25]. The results of this report reveal that FBXL20 can act as an effector for the p53 function in the suppression of PR55 $\alpha$  protein stability. Thus, loss of FBXL20 expression phenocopies the loss of p53 function, reducing PR55 $\alpha$ -ubiquitination and stabilizes PR55 $\alpha$  protein, while the two together do not produce additive effects (see Figs. 1–4). Consistently, biochemical studies reveal a physical interaction of PR55 $\alpha$  and FBXL20 *in vitro* and *in vivo* (See Fig. 5), which provides further evidence supporting PR55 $\alpha$  as a substrate of FBXL20, which is a recognizing component of the SCF-E3 ubiquitin ligase complexes that promote protein degradation [23,24]. Thus, these results suggest a novel mechanism of PR55 $\alpha$  inhibition that is based on the p53-controlled ubiquitin-proteasome degradation machinery. Future studies are needed to identify the ubiquitination sites and degrons targeted by the p53/FBXL20 axis in the PR55 $\alpha$  protein for this regulation.

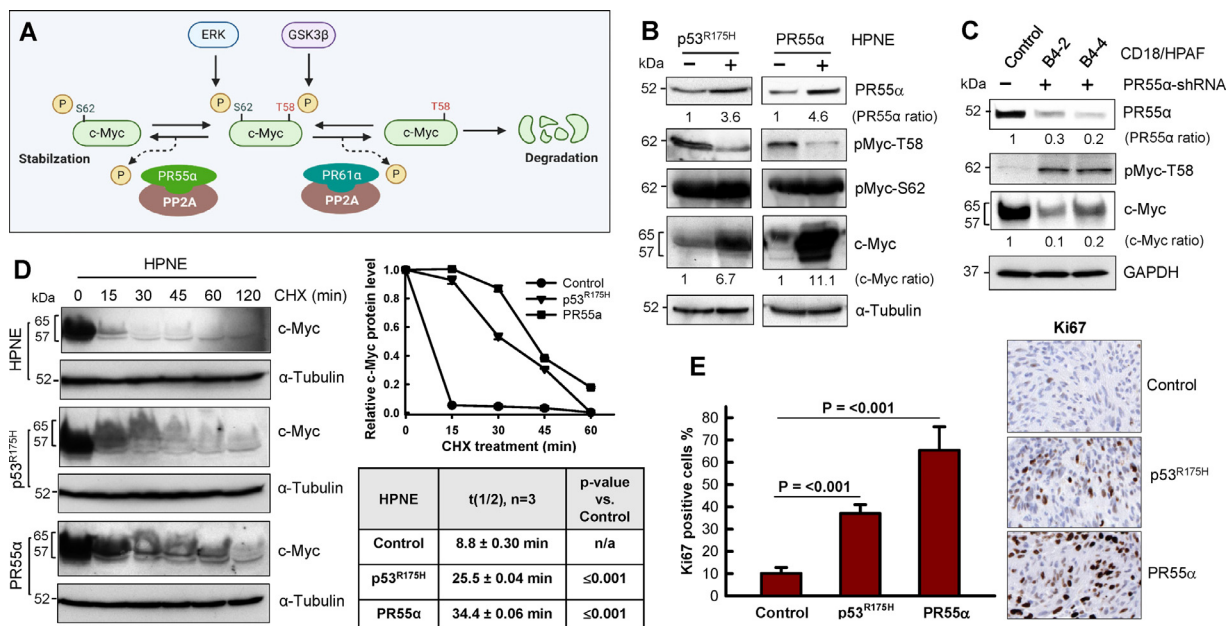


**Fig. 6.** Effect of p53 function and PR55 $\alpha$  expression on c-Myc protein stability. (A) c-Myc protein stability is regulated by phosphorylation [16,49,50,60]. While the phosphorylation of c-Myc-S62 by ERK kinase promotes c-Myc protein stability, the phosphorylation of c-Myc-T58 by GSK3 $\beta$  kinase facilitates c-Myc proteasomal degradation. In contrast, dephosphorylation of c-Myc-T58 is catalyzed by the PR55 $\alpha$ /PP2A complex to promote c-Myc stabilization, whereas dephosphorylation of c-Myc-S62 is by the PR61 $\alpha$ /PP2A complex to facilitate c-Myc proteasomal degradation. (B) HPNE/Control, HPNE/p53<sup>R175H</sup>, and HPNE/PR55 $\alpha$  (induction by 1 $\mu$ g/ml Dox for 3 days) cells were analyzed for the phosphorylation of c-Myc-T58 and c-Myc-S62, and total level of c-Myc by immunoblotting with antibodies against c-Myc-T58 (ab85380), c-Myc-S62 (33A12E10), and total c-Myc (D3N8F).  $\alpha$ -Tubulin served as an internal control. (C) CD18/HPAF pancreatic cancer cells were stably transduced with Dox-inducible control-shRNA or PR55 $\alpha$ -shRNA and incubated with 2  $\mu$ g/ml Dox for 3 days (for knocking down PR55 $\alpha$  levels). The cell lysates were analyzed by immunoblotting for the levels of PR55 $\alpha$ , phospho-Myc-T58, total c-Myc, and GAPDH. B4-2 and B4-4 are different PR55 $\alpha$ -shRNAs. (D) Effect of p53<sup>R175H</sup> and PR55 $\alpha$  on c-Myc protein stability. Left panel: The indicated cells were incubated with 15  $\mu$ g/ml CHX, to halt protein synthesis, for the indicated times and analyzed for c-Myc protein levels by immunoblotting. As a loading control,  $\alpha$ -tubulin was assessed by Western blot analysis. HPNE/PR55 $\alpha$  cells were induced for ectopic PR55 $\alpha$  expression by incubation with Dox (1 $\mu$ g/ml) for 3 days before CHX treatment. Right panel: Line-graph: the levels of c-Myc and  $\alpha$ -Tubulin on the blots were quantified using Fiji-ImageJ software, and relative c-Myc levels were determined by normalizing to  $\alpha$ -Tubulin levels. Bottom table: c-Myc protein half-life was calculated by linear regression analysis of log (c-Myc level) against time using SigmaPlot software. The data represent the mean $\pm$ S.D. of three independent experiments. (E) Effect of p53<sup>R175H</sup> mutant and PR55 $\alpha$  on anchorage-independent proliferation. HPNE/Control, HPNE/p53<sup>R175H</sup>, and HPNE/PR55 $\alpha$  cells were plated in 0.35% soft-agar with growth medium at 50K cells/well in 6-well plates for 3 weeks. Dox (1  $\mu$ g/ml) was added to the medium to maintain ectopic PR55 $\alpha$  expression in HPNE/PR55 $\alpha$  cells. The 3D-spheroids formed in soft-agar were harvested and embedded with Histogel (ThermoFisher) and analyzed for proliferation rate by quantifying the cells positive in Ki67 expression (ab16667, 1:200 dilution) by immunohistochemistry analysis (IHC), as instructed by the manufacturer. The Bar graph summarizes the Ki67 positive cells in the indicated samples and represents the mean $\pm$ S.D. (n=4). Right panel: Representative images show Ki67 positive cells in dark brown color in the 3D-spheroids.

Although PR55 $\alpha$  and FBXL20 are present in both the cytoplasm and nuclei, PR55 $\alpha$  expression is relatively higher in the nuclei (see Fig. 5). Ectopic PR55 $\alpha$  expression significantly increases the nuclear portion of PR55 $\alpha$  expression, which coincidentally associates with a reduced co-localization of PR55 $\alpha$  with FBXL20 (see Fig. 5C–E). Since several PR55 $\alpha$ -promoted oncoproteins (e.g.  $\beta$ -catenin, c-Myc, YAP) are transcription factors in the nuclei [12,15,17,50,57], inhibition of PR55 $\alpha$  by the p53/FBXL20 axis is anticipated to suppress these oncoproteins. Indeed, our previous studies show that PR55 $\alpha$  supports the activation of  $\beta$ -catenin and YAP [15,17], and current studies demonstrate that PR55 $\alpha$  promotes c-Myc protein stability, which is associated with concomitant dephosphorylation of c-Myc-T58, a substrate of PR55 $\alpha$  (see Fig. 6). Thus, these results implicate the inhibition of PR55 $\alpha$  as a new tumor suppressor function of p53.

Loss of p53 tumor suppressor is the most frequent event in human cancers. Deficiency in p53 function not only promotes malignant transformation, but also facilitates metastatic diseases of many solid tumor types including

those in the breast, lung, colorectal, and pancreas [59]. Inactivation of p53 is essential for pancreatic cancer to progress into invasive and metastatic diseases [19,21,22]. The studies in this report demonstrate a novel function of p53 in the inhibition of PR55 $\alpha$  expression, which supports several core oncogenic pathways, including YAP,  $\beta$ -catenin, ERK, and c-Myc that are critical for the oncogenesis and progression of pancreatic cancer [12,15,17,50,57]. Accordingly, our previous studies demonstrate that PR55 $\alpha$  is required for both *in vivo* tumorigenicity and metastasis of pancreatic cancer cells [15]. Consistent with the observed correlation between high-PR55 $\alpha$  levels with poor survival of pancreatic cancer patients [15], results in this report show that pancreatic cancer tissues express significantly lower levels of FBXL20 than normal tissues, and low-FBXL20 levels correlate with the poor survival of pancreatic cancer patients (See Fig. 7). Collectively, the studies in this report reveal a novel tumor suppression mechanism based on the p53/FBXL20 axis in the negative regulation of PR55 $\alpha$  protein stability and subsequent PR55 $\alpha$ -promoted c-Myc oncogenic pathway.

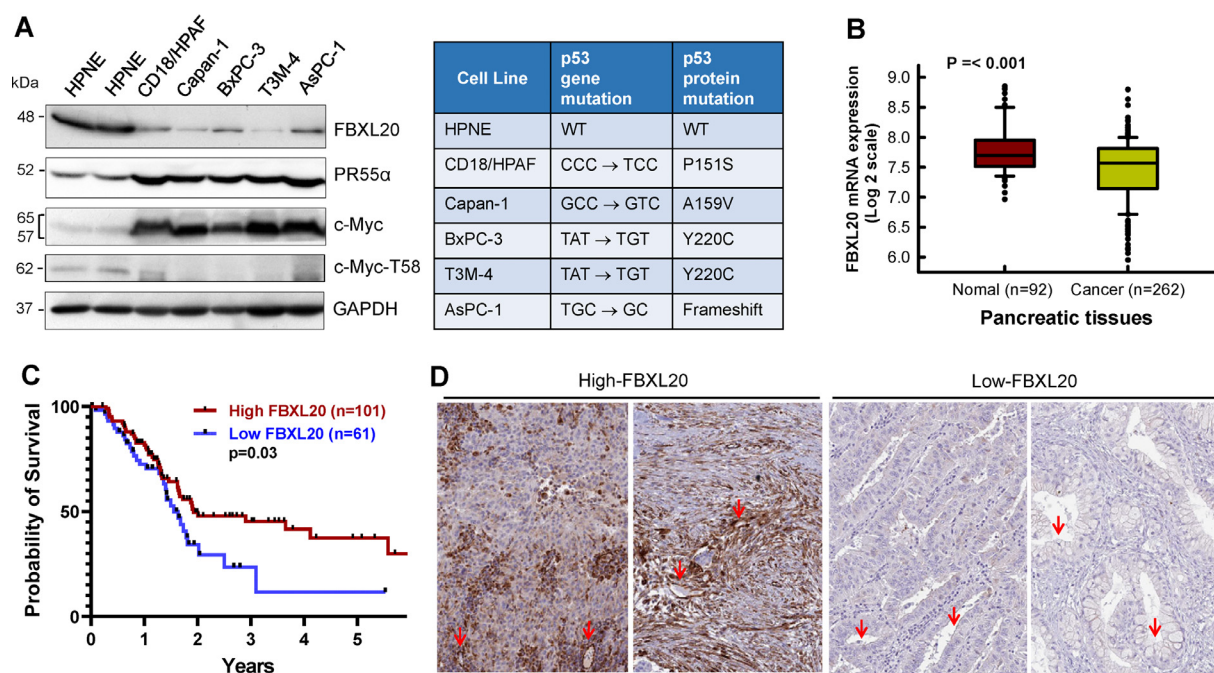


**Fig. 7.** FBXL20 levels are significantly lower in pancreatic cancer cells/tissues compared to normal cells/tissues and negatively associate with the survival of pancreatic cancer patients. (A) The indicated pancreatic normal and cancer cell lines were analyzed for the levels of FBXL20, PR55 $\alpha$ , c-Myc, c-Myc-T58, and GAPDH by Western blot analyses. The mutational status of p53 in the cell lines is described in the table [45]. (B) Box plot shows FBXL20 mRNA expression data for pancreatic cancer (n = 262) and normal tissues (n = 92) from the GENT2 database GPL570 platform (data set: HG-U133 Plus 2) [55]. (C) High levels of FBXL20 mRNA correlate with better survival of pancreatic cancer patients, as determined by Kaplan-Meier survival analysis. mRNA sequencing data of the pancreatic cancer specimens retrieved from the Human Protein Atlas data set [61] was plotted at high (n = 101) and low (n = 61) FBXL20 expression in association with patient survival. The mRNA level (FPKM)  $\geq$  2.3 was considered a high level of FBXL20 expression. Red and blue lines denote the cases expressing high and low FBXL20, respectively. (D) Representative images show high (left panels) and low (right panels) expression of FBXL20 by IHC. Arrows point to pancreatic ducts (For interpretation of the references to color in this figure legend, the reader is referred to the web version of this article.).

## Funding

This work was supported, in part, by NIH/NIGMS R01GM143329, NIH/NCI R01CA206444, U.S. Army/USAMRAA/CDMRP W81XWH2110700, Nebraska/DHHS (2022-59), Nebraska/DHHS (2022-42), University of Nebraska Collaboration Initiative Program Award (no number), a pilot project award by the Great Plains IDEa-CTR-Pilot Projects Program 5U54GM115458, and a pilot project award by the Nebraska Center for Cellular Signaling P30GM106397.

## Declaration of Competing Interest

The authors declare no conflict of interest.

## CRedit authorship contribution statement

**Lepaksh S.V. Madduri:** Investigation, Formal analysis, Writing – original draft. **Nichole D. Brandquist:** Investigation, Formal analysis, Writing – original draft. **Chitra Palanivel:** Conceptualization, Validation. **Geoffrey A. Talmon:** Formal analysis. **Michael J. Baine:** Software, Writing – review & editing. **Sumin Zhou:** Software, Writing – review & editing. **Charles A. Enke:** Software, Writing – review & editing. **Keith R. Johnson:** Data curation, Writing – review & editing. **Michel M. Ouellette:** Visualization, Software, Formal analysis. **Ying Yan:** Visualization, Supervision, Writing – original draft.

## Acknowledgments

We thank James Talaska and Janice Taylor for assistance with confocal microscopy [UNMC Microscope Core supported by NIGMS/P30GM106397], Dr. Robert Lewis for c-Myc-T58 and c-Myc-S62 antibodies, and Drs. Parthasarathy Seshacharyulu and Surinder Batra for the RT-PCR analysis of PR55 $\alpha$ -mRNA expression.

## Supplementary materials

Supplementary material associated with this article can be found, in the online version, at doi:10.1016/j.neo.2021.10.002.

## References

- [1] Eichhorn PJ, Creighton MP, Bernards R. Protein phosphatase 2A regulatory subunits and cancer. *Biochim Biophys Acta* 2009;1795:1–15.
- [2] Seshacharyulu P, Pandey P, Datta K, Batra SK. Phosphatase: PP2A structural importance, regulation and its aberrant expression in cancer. *Cancer Lett* 2013;335:9–18.
- [3] Janssens V, Longin S, Goris J. PP2A holoenzyme assembly: in cauda venenum (the sting is in the tail). *Trends Biochem Sci* 2008;33:113–21.
- [4] Ruvolo PP. The broken "Off" switch in cancer signaling: PP2A as a regulator of tumorigenesis, drug resistance, and immune surveillance. *BBA Clin* 2016;6:87–99.
- [5] Bikel I, Montano X, Agha ME, Brown M, McCormack M, Boltax J, Livingston DM. SV40 small t antigen enhances the transformation activity of limiting concentrations of SV40 large T antigen. *Cell* 1987;48:321–30.

- [6] Pallas DC, Shahrik LK, Martin BL, Jaspers S, Miller TB, Brautigam DL, Roberts TM. Polyoma small and middle T antigens and SV40 small t antigen form stable complexes with protein phosphatase 2A. *Cell* 1990;**60**:167–76.
- [7] Skoczylas C, Fahrbach KM, Rundell K. Cellular targets of the SV40 small-t antigen in human cell transformation. *Cell Cycle* 2004;**3**:606–10.
- [8] Sangodkar J, Farrington CC, McClinch K, Galsky MD, Kastrinsky DB, Narla G. All roads lead to PP2A: exploiting the therapeutic potential of this phosphatase. *FEBS J* 2016;**283**:1004–24.
- [9] Balmanno K, Cook SJ. Tumour cell survival signalling by the ERK1/2 pathway. *Cell Death Differ* 2008;**16**:368–77.
- [10] Zhang Y, Wang X. Targeting the Wnt/ $\beta$ -catenin signaling pathway in cancer. *J Hematol Oncol* 2020;**13**:165.
- [11] Stine ZE, Walton ZE, Altman BJ, Hsieh AL, Dang CV. MYC, Metabolism, and Cancer. *Cancer Discov* 2015;**5**:1024–39.
- [12] Adams DG, Coffee RL, Zhang H, Pelech S, Strack S, Wadzinski BE. Positive regulation of Raf1-MEK1/2-ERK1/2 signaling by protein serine/threonine phosphatase 2A holoenzymes. *J Biol Chem* 2005;**280**:42644–54.
- [13] Ory S, Zhou M, Conrads TP, Veenstra TD, Morrison DK. Protein phosphatase 2A positively regulates Ras signaling by dephosphorylating KSR1 and Raf-1 on critical 14-3-3 binding sites. *Curr Biol* 2003;**13**:1356–64.
- [14] MacDonald BT, Tamai K, He X. Wnt/ $\beta$ -catenin signaling: components, mechanisms, and diseases. *Dev cell* 2009;**17**:9–26.
- [15] Hein AL, Seshacharyulu P, Rachagani S, Sheinin YM, Ouellette MM, Ponnusamy MP, Mumby MC, Batra SK, Yan Y. PR55 $\alpha$  subunit of protein phosphatase 2A supports the tumorigenic and metastatic potential of pancreatic cancer cells by sustaining hyperactive oncogenic signaling. *Cancer Res* 2016;**76**:2243–53.
- [16] Farrell AS, Sears RC. MYC degradation. *Cold Spring Harb Perspect Med* 2014;**4**:a014365.
- [17] Hein AL, Brandquist ND, Ouellette CY, Seshacharyulu P, Enke CA, Ouellette MM, Batra SK, Yan Y. PR55 $\alpha$  regulatory subunit of PP2A inhibits the MOB1/LATS cascade and activates YAP in pancreatic cancer cells. *Oncogenesis* 2019;**8**:63.
- [18] Kasthuber ER, Lowe SW. Putting p53 in Context. *Cell* 2017;**170**:1062–78.
- [19] Gnoni A, Licchetta A, Scarpa A, Azzariti A, Brunetti AE, Simone G, Nardulli P, Santini D, Aieta M, Delcuratolo S, et al. Carcinogenesis of pancreatic adenocarcinoma: precursor lesions. *Int J Mol Sci* 2013;**14**:19731–62.
- [20] Mantovani F, Collavin L, Del Sal G. Mutant p53 as a guardian of the cancer cell. *Cell Death Differ* 2019;**26**:199–212.
- [21] Makohon-Moore A, Iacobuzio-Donahue CA. Pancreatic cancer biology and genetics from an evolutionary perspective. *Nat Rev Cancer* 2016;**16**:553–65.
- [22] Notta F, Hahn SA, Real FX. A genetic roadmap of pancreatic cancer: still evolving. *Gut* 2017;**66**:2170.
- [23] Kenzelmann Broz D, Spano Mello S, Biegging KT, Jiang D, Dusek RL, Brady CA, Sidow A, Attardi LD. Global genomic profiling reveals an extensive p53-regulated autophagy program contributing to key p53 responses. *Genes Dev* 2013;**27**:1016–31.
- [24] Yumimoto K, Yamauchi Y, Nakayama KI. F-box proteins and cancer. *Cancers (Basel)* 2020;**12**:1249.
- [25] Xiao J, Zhang T, Xu D, Wang H, Cai Y, Jin T, Liu M, Jin M, Wu K, Yuan J. FBXL20-mediated Vps34 ubiquitination as a p53 controlled checkpoint in regulating autophagy and receptor degradation. *Genes Dev* 2015;**29**:184–96.
- [26] Wong PM, Feng Y, Wang J, Shi R, Jiang X. Regulation of autophagy by coordinated action of mTORC1 and protein phosphatase 2A. *Nat Commun* 2015;**6**:8048.
- [27] Reid Michael A, Wang W-I, Rosales Kimberly R, Welliver Meng X, Pan M, Kong M. The B55 $\alpha$  subunit of PP2A drives a p53-dependent metabolic adaptation to glutamine deprivation. *Mol Cell* 2013;**50**:200–11.
- [28] Honarpour N, Rose CM, Brumbaugh J, Anderson J, Graham RL, Sweredoski MJ, Hess S, Coon JJ, Deshaies RJ. F-box protein FBXL16 binds PP2A-B55 $\alpha$  and regulates differentiation of embryonic stem cells along the FLK1+ lineage. *Mol Cell Proteom* 2014;**13**:780–91.
- [29] Lee KM, Nguyen C, Ulrich AB, Pour PM, Ouellette MM. Immortalization with telomerase of the Nestin-positive cells of the human pancreas. *Biochem Biophys Res Commun* 2003;**301**:1038–44.
- [30] Campbell PM, Groehler AL, Lee KM, Ouellette MM, Khazak V, Der CJ. K-Ras promotes growth transformation and invasion of immortalized human pancreatic cells by Raf and phosphatidylinositol 3-kinase signaling. *Cancer Res* 2007;**67**:2098–106.
- [31] Harvey DM, Levine AJ. p53 alteration is a common event in the spontaneous immortalization of primary BALB/c murine embryo fibroblasts. *Genes Dev* 1991;**5**:2375–85.
- [32] Nigro JM, Baker SJ, Preisinger AC, Jessup JM, Hosteller R, Cleary K, Signer SH, Davidson N, Baylin S, Devilee P, et al. Mutations in the p53 gene occur in diverse human tumour types. *Nature* 1989;**342**:705–8.
- [33] Choudhury AD, Xu H, Baer R. Ubiquitination and proteasomal degradation of the BRCA1 tumor suppressor is regulated during cell cycle progression. *J Biol Chem* 2004;**279**:33909–18.
- [34] Chen F, Zhang Z, Bower J, Lu Y, Leonard SS, Ding M, Castranova V, Piwnica-Worms H, Shi X. Arsenite-induced Cdc25C degradation is through the KEN-box and ubiquitin-proteasome pathway. *Proc Natl Acad Sci U S A* 2002;**99**:1990–5.
- [35] Yan Y, Black CP, Cao PT, Haferbier JL, Kolb RH, Spieker RS, Ristow AM, Cowan KH. Gamma-irradiation-induced DNA damage checkpoint activation involves feedback regulation between extracellular signal-regulated kinase 1/2 and BRCA1. *Cancer Res* 2008;**68**:5113–21.
- [36] Yan Y, Cao PT, Greer PM, Nagengast ES, Kolb RH, Mumby MC, Cowan KH. Protein phosphatase 2A has an essential role in the activation of gamma-irradiation-induced G2/M checkpoint response. *Oncogene* 2010;**29**:4317–29.
- [37] Yan Y, Shay JW, Wright WE, Mumby MC. Inhibition of protein phosphatase activity induces p53-dependent apoptosis in the absence of p53 transactivation. *J Biol Chem* 1997;**272**:15220–6.
- [38] Arnst JL, Hein AL, Taylor MA, Palermo NY, Contreras JI, Sonawane YA, Wahl AO, Ouellette MM, Natarajan A, Yan Y. Discovery and characterization of small molecule Rac1 inhibitors. *Oncotarget* 2017;**8**:34586–600.
- [39] Schindelin J, Arganda-Carreras I, Frise E, Kaynig V, Longair M, Pietzsch T, Preibisch S, Rueden C, Saalfeld S, Schmid B, et al. Fiji: an open-source platform for biological-image analysis. *Nat Methods* 2012;**9**:676–82.
- [40] Thomsen R, Christensen MH. MolDock: a new technique for high-accuracy molecular docking. *J Med Chem* 2006;**49**:3315–21.
- [41] Xie S, Bahl K, Reinecke JB, Hammond GRV, Naslavsky N, Caplan S. The endocytic recycling compartment maintains cargo segregation acquired upon exit from the sorting endosome. *Mol Biol Cell* 2016;**27**:108–26.
- [42] Batra SK, Castelino-Prabhu S, Wikstrand CJ, Zhu X, Humphrey PA, Friedman HS, Bigner DD. Epidermal growth factor ligand-independent, unregulated, cell-transforming potential of a naturally occurring human mutant EGFRvIII gene. *Cell Growth Differ* 1995;**6**:1251–9.
- [43] Foster SA, Demers GW, Etscheid BG, Galloway DA. The ability of human papillomavirus E6 proteins to target p53 for degradation *in vivo* correlates with their ability to abrogate actinomycin D-induced growth arrest. *J Virol* 1994;**68**:5698–705.
- [44] Boyer SN, Wazer DE, Band V. E7 protein of human papilloma virus-16 induces degradation of retinoblastoma protein through the ubiquitin-proteasome pathway. *Cancer Res* 1996;**56**:4620–4.
- [45] Berrozpe G, Schaeffer J, Peinado MA, Real FX, Perucho M. Comparative analysis of mutations in the p53 and K-ras genes in pancreatic cancer. *Int J Cancer* 1994;**58**:185–91.
- [46] Kittler R, Surendranath V, Heninger AK, Slabicki M, Theis M, Putz G, Franke K, Caldarelli A, Grabner H, Kozak K, et al. Genome-wide resources of endoribonuclease-prepared short interfering RNAs for specific loss-of-function studies. *Methods* 2007;**4**:337–44.
- [47] Miller DM, Thomas SD, Islam A, Muench D, Sedoris K. c-Myc and cancer metabolism. *Clin Cancer Res Off J Am Assoc Cancer Res* 2012;**18**:5546–53.
- [48] McAnulty J, DiFeo A. The molecular 'Myc-anisms' behind Myc-driven tumorigenesis and the relevant Myc-directed therapeutics. *Int J Mol Sci* 2020;**21**:9486.

- [49] Sears RC. The life cycle of C-myc: from synthesis to degradation. *Cell Cycle* 2004;**3**:1133–7.
- [50] Zhang L, Zhou H, Li X, Vartuli RL, Rowse M, Xing Y, Rudra P, Ghosh D, Zhao R, Ford HL. Eya3 partners with PP2A to induce c-Myc stabilization and tumor progression. *Nat Commun* 2018;**9**:1047.
- [51] Loukopoulos P, Kanetaka K, Takamura M, Shibata T, Sakamoto M, Hirohashi S. Orthotopic transplantation models of pancreatic adenocarcinoma derived from cell lines and primary tumors and displaying varying metastatic activity. *Pancreas* 2004;**29**:193–203.
- [52] Moore PS, Sipos B, Orlandini S, Sorio C, Real FX, Lemoine NR, Gress T, Bassi C, Klöppel G, Kalthoff H, et al. Genetic profile of 22 pancreatic carcinoma cell lines. *Virchows Archiv* 2001;**439**:798–802.
- [53] Deer EL, Gonzalez-Hernandez J, Coursen JD, Shea JE, Ngatia J, Scaife CL, Firpo MA, Mulvihill SJ. Phenotype and genotype of pancreatic cancer cell lines. *Pancreas* 2010;**39**:425–35.
- [54] Klauschen F, Wienert S, Schmitt WD, Loibl S, Gerber B, Blohmer JU, Huober J, Rüdiger T, Erbströßer E, Mehta K, et al. Standardized Ki67 diagnostics using automated scoring—clinical validation in the GeparTrio breast cancer study. *Clin Cancer Res* 2015;**21**:3651–7.
- [55] Park SJ, Yoon BH, Kim SK, Kim SY. GENT2: an updated gene expression database for normal and tumor tissues. *BMC Med Genom* 2019;**12**:101.
- [56] Uhlen M, Fagerberg L, Hallstrom BM, Lindskog C, Oksvold P, Mardinoglu A, Sivertsson A, Kampf C, Sjostedt E, Asplund A, et al. Proteomics. Tissue-based map of the human proteome. *Science* 2015;**347**:1260419.
- [57] Zhang W, Yang J, Liu Y, Chen X, Yu T, Jia J, Liu C. PR55 $\alpha$ , a regulatory subunit of PP2A, specifically regulates PP2A-mediated  $\beta$ -Catenin Dephosphorylation. *J Biol Chem* 2009;**284**:22649–56.
- [58] Macgregor-Das AM, Iacobuzio-Donahue CA. Molecular pathways in pancreatic carcinogenesis. *J Surg Oncol* 2013;**107**:8–14.
- [59] Tang Q, Su Z, Gu W, Rustgi AK. Mutant p53 on the path to metastasis. *Trends Cancer* 2020;**6**:62–73.
- [60] Gregory MA, Qi Y, Hann SR. Phosphorylation by glycogen synthase kinase-3 controls c-myc proteolysis and subnuclear localization. *J Biol Chem* 2003;**278**:51606–12.
- 61 Uhlen M, Zhang C, Lee S, Sjostedt E, Fagerberg L, Bidkhorji G, Benfeitas R, Arif M, Liu Z, Edfors F, et al. A pathology atlas of the human cancer transcriptome. *Science* 2017;**357**:eaan2507. doi:10.1126/science.aan2507.